

## **Chemistry of minerals and mass changes of elements during sodic-calcic alteration of the Panj-Kuh intrusive body (Damghan, Iran)**

**Maryam Sheibi**

*School of Earth Sciences, Shahrood University of Technology, Shahrood, Iran*

*e-mail: sheibi@shahroodut.ac.ir*

*(received: 22/10/2013 ; accepted: 06/07/2014)*

### **Abstract**

Exact petrography and mineral chemistry investigations of pristine and altered rocks of the post-Eocene Panj-Kuh pluton show that subsequent to emplacement and crystallization, rocks were subjected to two secondary composition equivalents, sodic-calcic and potassic alterations, respectively. Fresh rocks have syenitic composition and contain plagioclase (labradorite), K-feldspar, magmatic diopside, biotite and minor magnetite, sphene and apatite. The rocks, subjected to Na-Ca alteration, are characterized by a bleached appearance and in point of modal classification referred to as monzonite. Albitization of the corner of plagioclase ( $An_{10}Ab_{85}Or_5$ ), pervasive scapolitization of the plagioclases (marialite,  $Ma_{97}Me_2$ ) and albite with chessboard twinning are some common properties of rocks subjected by this type alteration. Magmatic magnetite is enclosed in pyroxene and biotite and is also dissolved and partially removed. This type of metasomatism is structurally controlled by fracturing, with filling minerals of albite, scapolite, analcime, clinopyroxene, sphene and apatite (scapolite-albite veins). The pyroxene has the same composition in syenites, monzonite and in scapolite-albite veins (on average,  $Wo_{48}En_{38}Fo_{12}$ ). This means that the secondary hydrothermal effects do not tend to alter the composition of primary clinopyroxene. The average Or content of potassium feldspar crystals in altered and unaltered rocks range from  $Or_{90}$  to  $Or_{84}$ . According to the isocon method and the obtained plots, Ti and REEs were relatively immobile during Na-Ca alteration and the mass change calculations varied from 1 to 20%, depending on the intensity of alteration. By contrast, the washed-out contents of K and Fe invaded the other rocks and created potassic zone alteration. These rocks were characterized by the conversion of magmatic pyroxene and biotite to shreddy biotite (with dark green pleochroism and secondary fine sphene), as well as plagioclase surrounded by rinds of potassium feldspar.

**Keywords:** *syenite, sodic-calcic and potassic alterations, mineral chemistry, mass transfer, Damghan, Iran*

### **Introduction**

The Panj-Kuh district, 50 km southeast of Damghan, is located in northeastern Iran. Fe oxide deposits are most commonly found in this area, the total reserves of which in the Panj-Kuh area are estimated to be 500 million tonnes of iron ore, with a general chemical composition of  $Fe_2O_3=84.2\%$ ,  $FeO=8.5\%$ . Ore deposits are commonly dominated by iron oxide (magnetite and/or hematite) and surrounded by a 100 to 500 meter halo of  $Na \pm Ca$  alteration. However, experimental, theoretical and field studies in other parts of world have shown systematic associations between the mineralogical and chemical composition of pluton and the metal content of associated skarn. Recent studies have presented well-defined connections between major metal types and various magmatic rocks ranging from granite to diorite (Carten, 1982; Meinert, 1995; Barton & Johnson, 2000). Since the geochemistry and mineralogy of the Panj-Kuh granitic rocks and their role in the petrogenesis of the ore deposit have not been previously investigated, this paper uses field relations, petrography and geochemistry data in the

evaluation of magmatic and fluid phases during the final stages of crystallization and cooling within the Panj-Kuh intrusive body. Mass changes in major and minor elements in the Panj-Kuh pluton are quantitatively evaluated. Grant's (1986) method is employed to calculate mass changes during alteration. The major and trace elements are used to establish bulk mass changes during Na-Ca alteration episodes. The mass of the components added to or removed from the rock as a result of interaction with hydrothermal fluids are determined by comparing the corrected analyses for the altered rocks with those of least-altered equivalents. This study provides insight into the processes that contribute to Fe oxide mineralization and sodic-calcic alteration and as such provides a record of the magmatic- to hydrothermal-transition during the crystallization of magmas.

### **Geological setting**

The Panj-Kuh district lies in the northern part of the structural zone of Central Iran. Based on regional tectonic considerations, Alavi (1972) suggested that the volcanic rocks in the adjacent

area were related to Eocene magmatic rocks of Central Iran to the south and not to the volcanic rocks of the Alborz magmatic belt to the west. The Panj-Kuh district consists mainly of igneous rocks of Tertiary. Structural patterns are controlled by two principal strike-slip faults, the Atary in the north and the Anjilow in the south, both with northeast trends.

An area of about 21 km<sup>2</sup> was mapped at Panj-Kuh (Fig. 1). Three main rock units occur in this area that, from oldest to youngest, comprise the following: volcanic rock from the Eocene, intrusive rock and Quaternary alluvial deposits (PIQ<sup>c</sup>, Qt1 and Qt<sup>2</sup>, Fig. 1). The volcanic outcrops consist mainly of andesitic breccia (Ev<sub>2</sub>), porphyritic trachyandesite lava, basalt, tuffaceous sandstone (E<sup>ta</sup>) and a thick-bedded volcanic sedimentary

sequence (E<sup>cs</sup>). These sequences were formed as a result of the alternation of conglomerate, a red to pink coarse sandstone in the basal section, followed by tuffaceous red shale and ultimately andesite, and trachybasalt in the upper section (E<sup>ab</sup>). Subordinate units of carbonated tuffaceous (L<sub>v</sub>) also occur in this area and are the main host of the Panj-Kuh iron mine. Volcanic rocks have also been intruded by intrusive rocks trending roughly N-S, with dimensions of 3.4 × 1.2 km<sup>2</sup>. Their ages are uncertain, possibly post-Eocene/early Oligocene, or much younger. Panj-Kuh granitoid rock is compositionally fractionated by pyroxene syenite to biotite syenite and is calc-alkaline and metaluminous in nature (Sheibi, 2003). Alluvial Quaternary deposits cover the southern and northern margins of the pluton (Fig. 1).

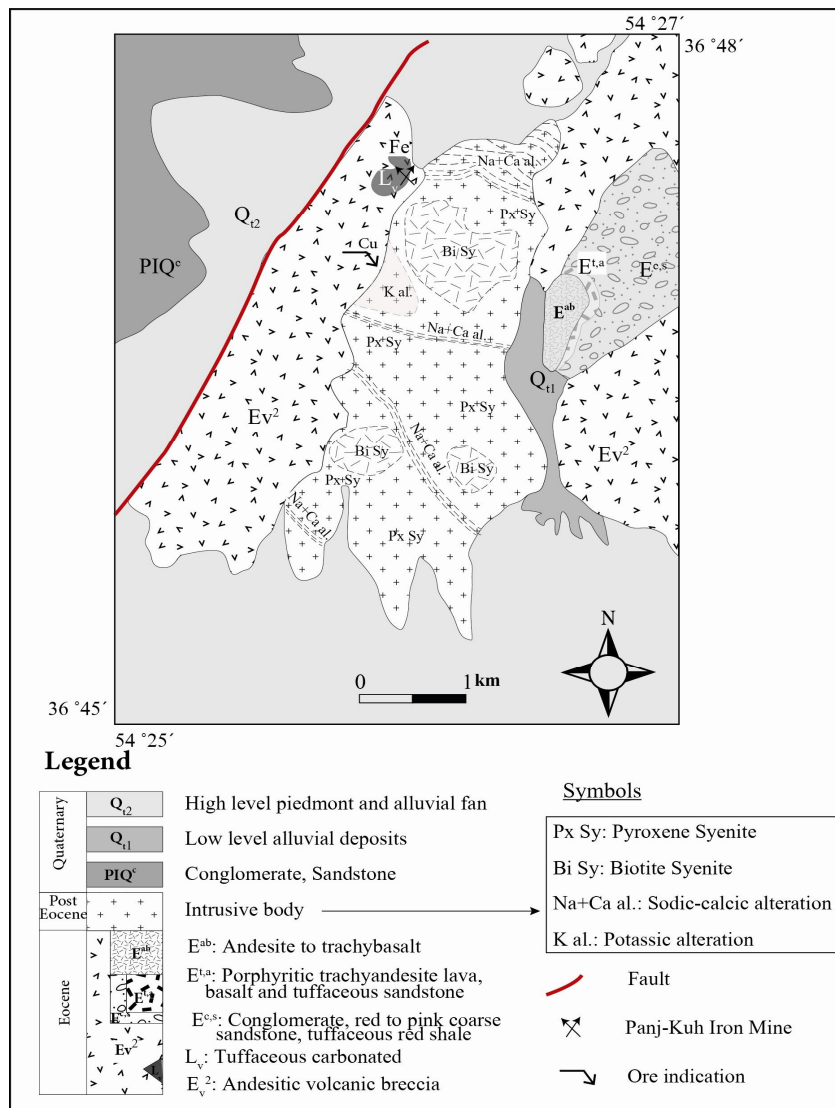


Figure 1: Simplified geological map of Panj-Kuh intrusive body (Sheibi, 2003)

## Methods

Fieldwork conducted for this study over a period of 20 days included collecting geological data and representative samples of different rock types and alteration zones. Texture and mineral relationships were examined in more than 100 thin sections from different parts of intrusive rock. Relationships between ore and gangue minerals were investigated using five and 25 thin-polished and polished sections, respectively.

In this study, 12 samples selected from Panj-Kuh intrusive rock were analysed. Precision was  $\pm 0.01$  wt. percentage. Trace elements, including the REE and high field strength elements (HFSE) were analysed using inductively coupled plasma mass spectrometry (ICP-MS) at the SGS Laboratory in Canada. Modal and chemical analyses of selected samples from different rock types are shown in separated Tables.

The chemical composition of minerals were determined by electron microprobe analysis at the CNR Institute for Geosciences and Earth Resources (IGG) laboratory, Padua (Italy), using a Cameca SX50 operating in wavelength dispersion mode at 15 kV and 20nA. Counting times were 10 s at the peak and 5 s at the background for major elements and 20 s at peak and 10 s at the background for minor elements. The following reference materials were used for calibration: periclase (Mg), magnetite (Fe), diopside (Si and Ca), chromite (Cr), corundum (Al), MnTiO<sub>3</sub> (Mn and Ti), albite (Na), orthoclase (K), apatite (P for F) and vanadinite (Cl). Some of the standards applied were taken from the Smithsonian Microbeam Standards.

X-ray counts were converted into oxide weight percentages using the PAP correction program (Pouchou and Pichoir, 1991). Analyses were precise to within  $\pm 2\%$  for major elements and  $\pm 3-5\%$  for minor elements. The results of the chemical analyses are reported in Table 2.

The crystal chemical formula of pyroxene was calculated on the basis of six oxygen atoms, following Papike (1969). Fe<sup>3+</sup> was calculated by stoichiometry according to Droop (1987). The unit formula of scapolite was calculated following Sokolova and Hawthorne (2008) by normalizing to 12T = (Si+Al) atoms per formula unit (apfu); CO<sub>2</sub> content was calculated assuming that the A site was fully occupied by Cl, SO<sub>4</sub> and CO<sub>3</sub>. With this assumption, CO<sub>3</sub> = 1 - (Cl+SO<sub>4</sub>). The meionite content of scapolite was Me% =  $100 * \Sigma(M^{2+}) / (\Sigma M^{2+})$

+ M<sup>1+</sup>). The unit formulae for feldspar, biotite and apatite were calculated on the basis of eight, 22 and 25 oxygen, respectively.

## Discussion

### Petrography

Based on field studies, petrography and geochemical data, three different types of igneous rocks were recognized in the Panj-Kuh intrusive body: pyroxene syenite, biotite syenite and altered igneous rock (monzonite) (Fig. 1). Pyroxene syenites that covered most parts and especially the margins of the intrusive body were light grey to green in colour, medium grained and granular in texture (Fig. 2a). These rocks consisted of 60-66% K-feldspar and 15-23% plagioclase, and were accompanied by 9-13% clinopyroxene (Table 1). Rare biotite (1-4%), magnetite (1.8-2.5), sphene (0.2-2.2%) and apatite (0.2-0.8%) also contributed to accessory minerals. Pyroxene crystals were subhedral to euhedral in shape, are pale green in colour and presented weakly pleochroic in plane-polarized light. Magnetite occurred as cubes and rounded cubes were included in pyroxene. Hence, it appears that they have magmatic origin. Most sphene crystals were euhedral in shape and displayed a wedge, diamond or lozenge shape.

Biotite syenites were compared with pyroxene syenites distributed as small patches in the central part of the outcrop (Fig. 1). In the field, biotite syenites have a darker colour due to the higher abundance of mafic components (especially biotites). These rock types are medium- to coarse-grained and consist of 75-85% K-feldspar, 5-7% plagioclase, 4-6% biotite and a lower amount of clinopyroxene (0.2-0.9%) (Fig. 2b). The K-feldspar occurred as large phenocrysts (up to 3 cm in diameter), giving rise to a porphyroitic texture (Fig. 2c). It also shows Carlsbad twinning and perthitic texture, which implies its magmatic origin (Fig. 2c). Biotites in coarse sheets surrounded clinopyroxene (Fig 2b). This mineral is magmatic in origin and commonly associated with pyroxene, magnetite, apatite, or sphene inclusions. Biotite also shows brown pleochroic and in some cases contained rutile needles, which confirmed its magmatic origin.

Despite the biotite and pyroxene syenites having the same mineral assemblages, the most obvious differences were related to their mineral sizes and abundances. A combination of the exact modal

analyses (Table 1) and a sampling map show that the average abundance of plagioclase decreased from 23% to 5%, clinopyroxene from 13% to 1%, subordinate opaque minerals from 2.2% to 0.5% and apatite from 0.8% to 0.2% from pyroxene syenites (in the margin) to biotite syenites (in the

centre). In contrast, K-feldspar increased from 60% to 85% and biotite from 1% to 6% (Table 1). These facts confirm the crystal fractionation process and the expectation of normal zonation in plutonic intrusive bodies.

Table 1: Modal analyses of different part of Panj-Kuh intrusive body. Bi-Sy: biotite syenite; Py-Sy: pyroxene syenite and M: monzonite. Abbreviations are after Kretz (1983).

S	Kfs	Pl	Scp	Cpy	Bt	Act	Spn	Ap	Mag	Qtz
Bi-Sy-1	85.5	5.3	-	0.9	6.1	1.4	0.4	0.3	1.1	-
Bi-Sy-2	81.3	6.7	-	0.3	4.1	1.4	1.2	0.3	3.8	-
Bi-Sy-3	82.9	6.3	-	0.6	5.4	4.0	0.2	0.3	1.9	-
Bi-Sy-4	84.0	5.2	-	0.8	5.4	2.3	0.2	0.2	1.2	-
Bi-Sy-5	75.8	6.4	-	0.2	-	2.4	0.4		0.4	13.0
Py-Sy-6	60.3	22.1	-	10.0	4.7	-	0.2	0.8	1.8	-
Py-Sy-7	63.1	22.7	-	7.5	2.2	-	0.2	0.2	2.5	-
Py-Sy-8	63.0	21.0	-	9.0	3.0	-	0.3	0.8	2.1	-
Py-Sy-9	62.0	22.0	-	11.2	2.3	-	0.4	0.8	2.4	-
Py-Sy-10	66.4	15.1	-	13.2	1.3	-	0.6	0.8	2.3	-
M-11	57.0	12.0	15.0	14.0	-	-	2.2	0.6	-	-
M-12	50.0	11.0	30.0	13.2	-	-	2.1	0.6	-	-
M-13	52.0	10.0	27.0	12.2	-	-	1.8	0.4	-	-
M-14	45.0	8.0	25.0	11.5	-	-	2.0	0.8	-	-
M-15	45.0	9.8	29.9	11.2	-	-	1.4	0.5	-	-
M-16	50.0	2.6	30.7	13.6	-	-	2.2	0.7	-	-
M-17	60.0	12.7	10.0	13.0	-	0.1	3.0	0.1	-	-

Alongside these two rock types, there is a third group that has been created by extensive sodic-calcic alteration on fresh rocks. This group is especially distributed in the northeastern margin of the pluton and as corridors cross-cutting the central parts of the body (Fig. 1, Na+Ca al.). In the field and under the microscope, these rocks show a bleached appearance and biotite and magnetite are rare or absent. These rocks have a light grey to white colour, are fine- to medium- grained and granular in texture. They consist essentially of K-feldspar (on average 51%), plagioclase (9.5%), scapolite (24%) and clinopyroxene (13%), with accessory minerals including sphene (2.1%) and apatite (0.5%) (Table 1; Figs. 2d, e, f and g). These rock types are modally referred to as monzonite, owing to high abundance of scapolite. The K-feldspar is medium- to coarse-grained. In some cases, cleavage traces have been preserved and display chessboard twinning, which is representative of the albitization of K-feldspar (Gilluly, 1993) (Fig. 2f). Plagioclase is fine- to medium-grained and euhedral to subhedral. Albitization of the corner of plagioclase (Fig. 2d),

widespread scapolitization of the plagioclases (Fig. 2e) and albite with chessboard twinning are among the common characteristics of these rock types in the Panj-Kuh pluton. Scapolite that is observed only in Na-Ca-altered rocks occurs in two forms: as a pervasive replacement of plagioclase in monzonite (Fig. 2e) and as a fracture-filling mineral with clinopyroxene, albite, analcime, sphene and apatite in scapolite veins (Fig. 2g). The rocks in the former case exhibited an igneous texture (granular) and with increasing scapolitization conversion to a rosette or poikiloblastic texture. Scapolite veins had concentrated to the northern margin of the intrusive body, especially when in contact with volcanic rocks (around the iron ore body). Their widths varied from a few millimetres to more than 500 metres (scapolite-albite skarn). These observations strongly suggest that scapolite poikiloblasts are not magmatic, but hydrothermal in origin.

In the west-end of the pluton map, for some samples, plagioclases were petrographically and locally surrounded by secondary K-feldspar and shreddy biotites containing small pieces of sphene (Fig. 1, K al.). In these rocks, carlsbad twinning was

observed in the corners of plagioclase (Fig. 2h) and most clinopyroxenes have converted to fine grain biotites (Fig. 2i). This type of biotites display commonly pale green and brown pleochroic in thin sections, ragged in shape and formed shreds, flakes and patchwork aggregates, and were accompanied by secondary fine sphene. In fact, these samples contained hydrothermal biotite only or combinations of magmatic and hydrothermal biotites. Dilles (1984) believed these aggregates of biotite had a low potassium content and atomic Fe/(Fe+Mg). On the other hand, Van Middelaar and

Keith (1990) believed in the migration and mobility of Ti during Na-Ca alteration. Thus, it seems that a portion of TiO<sub>2</sub> content in biotites have generated sphene during conversion to secondary shreddy biotite. These petrographic confirmations show that pyroxene and biotite syenites in the specified locations had been subjected to potassic alteration. Local occurrence of copper carbonates was also observed as quartz stockwork at these stations and especially in the adjacent volcanic rocks.

Table 2: The electron microprobe analyses of some mineral compositions from the fresh to intense sodic-calcic altered rocks of Panj-Kuh pluton. a) Feldspar, b) Scapolite, c) Biotite, d) Pyroxene, e) Magnetite, f) Apatite. \* #1: biotite syenite, #2: monzonite, #3: scapolite-albite vein

Sample number	#1					#2						
	Pl1	Pl2core	Pl2rim	Ab	Kf	Pl1core	Pl1rim	Pl2core	Pl2middle	Pl2rim	Kf1	Kf2
SiO <sub>2</sub>	54.73	57.47	60.97	65.61	64.94	58.78	62.90	56.62	60.53	61.12	64.55	63.55
Al <sub>2</sub> O <sub>3</sub>	28.32	26.16	24.21	21.24	18.21	25.76	22.72	26.40	24.35	23.68	20.03	19.58
Fe <sub>2</sub> O <sub>3</sub>	0.41	0.34	0.36	0.17	0.15	0.42	0.17	0.35	0.29	0.26	0.12	0.03
CaO	10.70	8.13	5.72	2.14	0.07	7.55	4.17	8.97	6.57	6.05	1.41	0.92
Na <sub>2</sub> O	5.57	6.71	8.16	10.01	1.70	7.05	8.98	6.52	7.61	8.15	3.73	3.29
K <sub>2</sub> O	0.23	0.28	0.47	0.82	14.02	0.42	0.65	0.19	0.37	0.42	9.94	10.85
Sum	99.96	99.08	99.89	100.07	99.09	100.02	99.59	99.04	99.74	99.68	99.78	98.27
<b>Structural formula based on 32 Oxygen</b>												
Si	2.47	2.60	2.72	2.89	3	2.63	2.80	2.57	2.70	2.73	2.93	2.94
Al	1.51	1.39	1.27	1.10	0.99	1.36	1.19	1.41	1.28	1.25	1.07	1.07
Fe	0.01	0.01	0.01	0.01	0.01	0.01	0.01	0.01	0.01	0.01	0	0
Ca	0.52	0.39	0.27	0.10	0	0.36	0.20	0.44	0.31	0.29	0.07	0.05
Na	0.49	0.59	0.70	0.86	0.15	0.61	0.77	0.57	0.66	0.71	0.33	0.30
K	0.01	0.02	0.03	0.05	0.83	0.02	0.04	0.01	0.02	0.02	0.58	0.64
Ab %	47.87	58.92	70.14	85.29	15.54	61.31	76.69	56.23	66.26	69.23	33.73	30.09
An %	50.82	39.47	27.19	10.09	0.35	36.28	19.67	42.72	31.61	28.41	7.06	4.66
Or %	1.32	1.61	2.66	4.62	84.11	2.42	3.64	1.05	2.13	2.36	59.22	65.25

#3						
Pl1	Pl2	Pl3	Kf1	Kf2	Kf3	Kf4
58.08	58.83	62.80	65.73	65.01	64.80	65.28
25.53	25.28	23.24	17.97	17.99	18.26	18.07
0.26	0.32	0.34	0.05	0.11	0.02	0.04
7.98	7.76	4.85	0	0.05	0	0
6.90	7.63	8.92	1.17	0.74	0.36	0.43
0.30	0.26	0.31	14.49	15.05	15.79	15.50
99.04	100.12	100.50	99.49	98.96	99.28	99.31
<b>Structural formula based on 32 Oxygen</b>						
2.62	2.63	2.77	3.03	3.02	3.01	3.02
1.36	1.33	1.21	0.98	0.98	1	0.99
0.01	0.01	0.01	0	0	0	0
0.39	0.37	0.23	0	0	0	0
0.60	0.66	0.76	0.10	0.07	0.03	0.04
0.02	0.01	0.02	0.85	0.89	0.93	0.92
59.97	63.12	75.56	10.97	6.91	3.39	4.04
38.31	35.47	22.71	0	0.26	0	0
1.72	1.41	1.73	89.03	92.83	96.61	95.96

Table 2b: Scapolite from #3

	Sc1	Sc3	4Sc5	4Sc6	4Sc7	4Sc8	Sc9	Sc10
SiO <sub>2</sub>	57.02	57.27	57.36	57.32	57.34	57.22	57.25	57.88
TiO <sub>2</sub>	0.01	0	0	0	0.04	0	0	0.01
Al <sub>2</sub> O <sub>3</sub>	22.33	22.37	23.72	22.80	23.45	22.56	21.64	22.59
Cr <sub>2</sub> O <sub>3</sub>	0.03	0	0	0	0.06	0.02	0.03	0.02
FeO	0.05	0.40	0.03	0.06	0.02	0.02	0.05	0.11
MgO	0.02	0.51	0.01	0	0.01	0.03	0	0.03
CaO	1.67	1.93	0.59	2.37	0.82	2.39	5.27	2.29
Na <sub>2</sub> O	12.37	11.19	12.62	12.05	12.30	11.91	10.70	11.30
K <sub>2</sub> O	0.49	0.49	0.14	0.53	0.24	0.64	1.22	0.54
F	0	0.01	0	0.02	0	0.04	0.03	0
Cl	1.28	1.37	0.48	1.57	0.62	1.65	3.93	1.69
SO <sub>3</sub>	0	0.02	0.03	0.04	0.05	0	0.02	0
P <sub>2</sub> O <sub>5</sub>	0.10	0.03	0.02	0.01	0.03	0.05	0.09	0.03
O=F,Cl	-0.29	-0.32	-0.11	-0.36	-0.14	-0.39	-0.90	-0.38
CO <sub>2</sub> calculated	3.406	3.300	4.404	3.091	4.212	2.997	0.162	2.978
Sum	98.47	98.58	99.29	99.50	99.05	99.14	99.49	99.10
<b>Structural formula based on 12 (Si +Al)</b>								
Si	8.210	8.218	8.068	8.170	8.097	8.193	8.302	8.220
Ti	0.1	0.0	0.0	0.0	0.4	0.0	0.0	0.1
Al	3.790	3.782	3.932	3.830	3.903	3.807	3.698	3.780
Cr	0.3	0.0	0.0	0.0	0.7	0.2	0.4	0.2
Fe	0.6	0.048	0.4	0.7	0.2	0.2	0.6	0.014
Mn	0.0	0.0	0.0	0.0	0.0	0.0	0.0	0.0
Mg	0.4	0.109	0.2	0.0	0.3	0.6	0.1	0.6
Ca	0.257	0.297	0.089	0.362	0.124	0.367	0.819	0.349
Na	3.453	3.113	3.442	3.329	3.367	3.305	3.8	3.112
K	0.090	0.090	0.024	0.097	0.044	0.118	0.225	0.098
F	0.0	0.5	0.0	0.7	0.0	0.018	0.015	0.0
Cl	0.312	0.334	0.113	0.378	0.149	0.400	0.966	0.406
S	0.0	0.2	0.3	0.5	0.5	0.0	0.2	0.0
P	0.012	0.3	0.2	0.2	0.4	0.6	0.011	0.3
Totale	16.138	16.2	15.680	16.187	15.708	16.224	17.056	15.991
C = 1-(Cl+S)	0.688	0.664	0.883	0.617	0.846	0.600	0.032	0.594
% Meionite (100Ca/Ca+Na)	7.02	12.43	2.68	9.72	3.64	9.89	20.35	10.30
%Marialite	92.98	87.57	97.32	90.28	96.36	90.11	79.65	89.70

Table 2c: Biotite

	#1					
	Bt1	Bt2	Bt3	Bt4	Bt5	Bt6
Na <sub>2</sub> O	0.25	0.21	0.15	0.16	0.35	0.23
MgO	12.73	12.81	12.55	12.46	12.33	12.71
Al <sub>2</sub> O <sub>3</sub>	13.72	13.74	13.64	13.78	13.69	13.65
SiO <sub>2</sub>	35.98	36.14	36.57	36.41	35.98	36.65
K <sub>2</sub> O	9.18	8.95	8.99	9.18	9.04	9.16
CaO	0.06	0.06	0.02	0	0.03	0.02
TiO <sub>2</sub>	4.65	4.70	4.39	4.89	6.07	5.04
Cr <sub>2</sub> O <sub>3</sub>	0.04	0.04	0	0	0.03	0.01
MnO	0.22	0.17	0.14	0.10	0.16	0.17
FeO	19.29	18.74	19.18	19.80	19.38	18.82
Sum	96.13	95.58	95.63	96.78	97.06	96.46
<b>Structural formula based on 22 oxygen</b>						
Si	5.469	5.498	5.563	5.496	5.415	5.525
Ti	0.531	0.538	0.502	0.555	0.687	0.572
Al	2.458	2.464	2.446	2.451	2.428	2.425
Cr	0.5	0.5	0.0	0.0	0.4	0.1
Fe	2.453	2.385	2.440	2.499	2.439	2.372
Mn	0.029	0.022	0.018	0.013	0.020	0.021
Mg	2.886	2.906	2.845	2.804	2.765	2.856
Ca	0.011	0.010	0.3	0.0	0.5	0.3
Na	0.074	0.061	0.044	0.047	0.101	0.069
K	1.779	1.738	1.745	1.768	1.735	1.761
#Mg	0.54	0.55	0.54	0.53	0.53	0.55
#Fe	0.46	0.45	0.46	0.47	0.47	0.45

Table 2d: Pyroxene

#1								
	Px5	Px6	Px7	Px8	Px11	Px12	Px13	Px14
SiO <sub>2</sub>	53.17	52.17	52.62	51.88	51.28	51.65	52.69	52.65
TiO <sub>2</sub>	0.11	0.21	0.03	0.09	0.10	0.11	0.16	0.05
Al <sub>2</sub> O <sub>3</sub>	0.73	0.98	0.28	0.30	0.65	0.68	0.70	0.37
Cr <sub>2</sub> O <sub>3</sub>	0.04	0.02	0	0	0	0.03	0	0
FeO	8.70	9.84	10.29	10.13	9.76	9.53	9.44	9.66
MnO	0.68	0.76	0.35	0.60	0.58	0.61	0.43	0.57
MgO	13.37	13.35	12.72	12.42	13.38	13.30	13.25	12.36
CaO	23.21	23.17	24.04	23.37	23.68	23.59	23.16	23.84
Na <sub>2</sub> O	0.48	0.43	0.39	0.22	0.34	0.41	0.47	0.36
K <sub>2</sub> O	0.01	0	0.01	0.02	0.02	0.02	0	0.01
Sum	100.49	100.94	100.72	99.04	99.79	99.92	100.30	99.88
Structural formula based on 6 oxygen. Fe <sup>3+</sup> calculated based on charge balance								
Si	1.974	1.933	1.961	1.971	1.921	1.932	1.963	1.980
Ti	0.3	0.6	0.1	0.3	0.3	0.3	0.5	0.1
Al	0.032	0.043	0.012	0.013	0.029	0.030	0.031	0.016
Cr	0.1	0.1	0.0	0.0	0.0	0.1	0.0	0.0
Fe <sup>3+</sup>	0.047	0.109	0.094	0.057	0.149	0.130	0.068	0.048
Fe <sup>2+</sup>	0.223	0.196	0.227	0.265	0.157	0.168	0.226	0.256
Mn	0.021	0.024	0.011	0.019	0.018	0.019	0.014	0.018
Mg	0.740	0.738	0.707	0.703	0.747	0.742	0.736	0.693
Ca	0.923	0.920	0.960	0.951	0.950	0.945	0.924	0.960
Na	0.034	0.031	0.028	0.016	0.025	0.029	0.034	0.026
K	0.0	0.0	0.1	0.1	0.1	0.1	0.0	0.1
Wo	46.92	46.15	47.63	47.73	46.86	46.92	46.50	48.42
En	37.61	37	35.07	35.30	36.84	36.82	37.01	34.93
Fs	13.72	15.30	15.92	16.14	15.08	14.80	14.80	15.32
# Mg	73.27	70.74	68.78	68.62	70.96	71.32	71.44	69.51

	#2							#3							
	Px1	Px2	Px3	Px4	Px13	Px14	Px15	7-Px1	7-Px2	7-Px3	7-Px4	5-Px3	5-Px4	5-Px5	5-Px6
SiO <sub>2</sub>	53.03	52.83	53.51	53.40	52.89	53.10	52.59	51.23	51.63	52.78	52.22	52.43	52.26	52.05	52.15
TiO <sub>2</sub>	0.10	0.06	0.05	0.04	0.04	0.05	0.09	0.26	0.03	0	0.08	0.10	0.03	0.07	0
Al <sub>2</sub> O <sub>3</sub>	0.58	0.29	0.14	0.75	0.35	0.34	0.42	1	0.34	0.21	0.48	0.57	0.28	0.33	0.28
Cr <sub>2</sub> O <sub>3</sub>	0.01	0.03	0	0.02	0.03	0	0	0.03	0.08	0.04	0	0.05	0	0	0.04
FeO	8.17	8.01	9.10	7.17	8.15	8.04	8.42	9.46	9.47	8.17	8.27	7.92	8.49	8.09	9.04
MnO	0.24	0.17	0.22	0.18	0.19	0.25	0.72	0.24	0.20	0.25	0.48	0.32	0.21	0.31	0.25
MgO	13.74	14.23	13.30	14.33	14.22	14.24	13.78	13.15	13.18	14.20	14.41	14.71	13.71	14.51	13.88
CaO	23.76	24.15	24.58	23.70	24.09	24.35	23.70	23.45	23.86	24.45	23.88	23.91	24.22	24.26	23.88
Na <sub>2</sub> O	0.28	0.36	0.19	0.23	0.25	0.27	0.22	0.52	0.41	0.25	0.37	0.32	0.26	0.26	0.32
K <sub>2</sub> O	0	0	0.02	0.01	0.01	0	0	0	0.02	0	0	0	0	0.05	0.03
Sum	99.91	100.13	101.12	99.84	100.22	100.65	99.93	99.34	99.21	100.35	100.19	100.32	99.45	99.92	99.88
Structural formula based on 6 oxygen. Fe <sup>3+</sup> calculated based on charge balance															
Si	1.977	1.959	1.980	1.983	1.962	1.961	1.963	1.925	1.944	1.956	1.935	1.937	1.958	1.933	1.945
Ti	0.3	0.2	0.2	0.1	0.1	0.2	0.2	0.7	0.1	0.0	0.2	0.3	0.1	0.2	0.0
Al	0.025	0.012	0.6	0.033	0.015	0.015	0.018	0.044	0.015	0.9	0.021	0.025	0.012	0.014	0.012
Cr	0.0	0.1	0.0	0.1	0.1	0.0	0.0	0.1	0.2	0.1	0.0	0.1	0.0	0.0	0.1
Fe <sup>3+</sup>	0.036	0.091	0.045	0.014	0.076	0.080	0.066	0.128	0.124	0.096	0.131	0.117	0.090	0.137	0.121
Fe <sup>2+</sup>	0.219	0.157	0.237	0.208	0.176	0.168	0.196	0.169	0.174	0.157	0.125	0.128	0.176	0.114	0.161
Mn	0.7	0.5	0.7	0.6	0.6	0.8	0.023	0.8	0.7	0.8	0.015	0.010	0.7	0.010	0.8
Mg	0.763	0.787	0.734	0.793	0.786	0.784	0.767	0.736	0.740	0.784	0.796	0.810	0.766	0.803	0.772
Ca	0.949	0.959	0.975	0.943	0.957	0.964	0.948	0.944	0.963	0.971	0.948	0.947	0.972	0.965	0.954
Na	0.020	0.026	0.014	0.017	0.018	0.020	0.016	0.038	0.030	0.018	0.026	0.023	0.019	0.019	0.023
K	0.0	0.0	0.1	0.0	0.0	0.0	0.0	0.0	0.1	0.0	0.0	0.0	0.0	0.2	0.2
Wo	47.75	47.48	48.65	47.73	47.53	47.82	47.56	46.84	47.41	47.91	46.78	46.77	48.06	47.35	46.97
En	38.41	38.94	36.62	40.15	39.04	38.89	38.47	36.54	36.43	38.71	39.28	40.03	37.86	39.40	38
Fs	12.82	12.30	14.05	11.27	12.55	12.32	13.18	14.75	14.68	12.50	12.64	12.09	13.15	12.32	13.88
# Mg	74.97	76	72.27	78.08	75.67	75.94	74.48	71.24	71.27	75.59	75.66	76.80	74.23	76.18	73.25

Table 2e: Magnetite

	#1							#2			#3	
	Ilm1	Ilm2	Mt1	Mt3	Mt4	Mt5	Mt6	Mt2	Mt3	Mt1	Mt1	Mt2
<b>MgO</b>	0.25	0.17	0.08	0.04	0.05	0.09	0.08	0.07	0.48	0.06	0.16	0.09
<b>Al<sub>2</sub>O<sub>3</sub></b>	0.02	0.02	0.30	0.52	0.37	0.35	0.47	0.22	0.57	0.26	0.28	0.25
<b>SiO<sub>2</sub></b>	0.16	0.16	0.25	0.31	0.16	0.22	0.23	0.55	1.71	0.33	0.38	0.24
<b>CaO</b>	0.01	0	0.10	0.01	0.03	0.05	0.03	0.37	0.69	0.15	0.05	0.07
<b>TiO<sub>2</sub></b>	48.79	48.25	1.35	1.78	1.98	2.41	2.10	0.76	1.35	1.17	0.41	0.25
<b>Cr<sub>2</sub>O<sub>3</sub></b>	0	0.07	0.02	0.07	0.02	0.04	0.04	0.17	0.03	0.16	0.29	0.33
<b>MnO</b>	2.69	2.76	0.22	0.28	0.27	0.18	0.25	0.21	0.35	0.33	0.10	0.09
<b>FeO</b>	48.74	47.98	91.30	90.52	91.64	90.53	91.47	88.80	87	90.29	89.79	90.37
<b>Sum</b>	100.65	99.41	93.62	93.52	94.52	93.87	94.66	91.15	92.19	92.76	91.46	91.70

Table 2f: Apatite.

	#1			#2		#3			
	Ap1	Ap3	Ap6	Ap1	Ap6	Ap1	Ap7	Ap8	Ap9
<b>SiO<sub>2</sub></b>	0.47	0.34	0.35	0.23	0.18	0.35	0.24	0.43	0.12
<b>TiO<sub>2</sub></b>	0.03	0	0.02	0	0.02	0	0	0.01	0.02
<b>Al<sub>2</sub>O<sub>3</sub></b>	0	0	0	0	0	0	0	0	0
<b>Cr<sub>2</sub>O<sub>3</sub></b>	0	0	0.01	0.05	0	0.08	0	0	0
<b>FeO</b>	0.08	0.23	0.09	0.07	0.03	0.09	0.06	0.03	0.11
<b>MnO</b>	0.07	0.07	0.08	0.08	0.07	0.04	0.03	0.04	0
<b>MgO</b>	0.02	0	0	0	0	0	0	0	0.01
<b>CaO</b>	54.02	53.92	54.22	54.73	54.53	53.64	54.85	54.17	55
<b>Na<sub>2</sub>O</b>	0.02	0.04	0.09	0.02	0.03	0.06	0	0.09	0
<b>K<sub>2</sub>O</b>	0	0	0.04	0.02	0.01	0	0	0	0
<b>F</b>	4.66	4.78	5.11	4.94	5.18	4.98	4.99	4.59	4.70
<b>Cl</b>	0.96	0.78	0.80	0.77	0.72	1	0.88	0.82	0.74
<b>SO<sub>3</sub></b>	0.11	0.15	0	0.04	0.01	0.03	0	0.13	0.03
<b>P<sub>2</sub>O<sub>5</sub></b>	42.78	42.18	43.42	42.83	43.69	42.97	43.09	42.15	43.04
<b>O=F,Cl</b>	-2.18	-2.19	-2.33	-2.26	-2.34	-2.32	-2.30	-2.12	-2.14
<b>Sum</b>	<b>101</b>	<b>100</b>	<b>102</b>	<b>102</b>	<b>102</b>	<b>101</b>	<b>102</b>	<b>100</b>	<b>102</b>

### Mineral chemistry

Electron microprobe analyses determined the chemistry of minerals from each of the identified mineral assemblages. Three polished-thin sections were selected as representative samples of the fresh intrusive rocks, alongside rocks that had undergone strong sodic-calcic alteration. Sample one was biotite syenite and was the least altered; samples two and three were representative of intrusive rocks that have undergone moderate and intense sodic-calcic alteration, respectively. The latter samples were labelled monzonite and scapolite-albite vein, respectively. Below, some of the most important differences in the petrography and mineral chemistry of the mentioned rock types are discussed.

### Feldspars

In total, 59 analyses were completed from three separate samples (one fresh biotite syenite and two rocks that were subjected to moderate and intense

sodic-calcic alteration). These included 55 plagioclase and four K-feldspar analyses. The selected analyses from these samples are summarized in Table 2a and the following results were obtained according to the rock composition. Some plagioclases from biotite syenite had higher calcic components (labradorite) within the core (e.g., An<sub>51</sub>Ab<sub>48</sub>Or<sub>1</sub>, Table 3, Fig. 3a). In this sample (#1), the composition of another plagioclase changed from An<sub>40</sub>Ab<sub>59</sub>Or<sub>2</sub> in the core to An<sub>27</sub>Ab<sub>70</sub>Or<sub>3</sub> in the rim (Table 2, Fig. 3a). Fine-grained plagioclase crystals were observed as inclusions within the larger K-feldspar with a composition of An<sub>0.5</sub>Ab<sub>15</sub>Or<sub>84</sub> (Table 2a, Fig. 3a). In monzonites and additionally altered rocks (samples 2 and 3, as shown in Figure 4 and Table 2), the average compositions of plagioclase in the core and rim were An<sub>42</sub>Ab<sub>56</sub>Or<sub>1</sub> and An<sub>20</sub>Ab<sub>77</sub>Or<sub>3</sub>, respectively. In these rocks, plagioclase continued with a narrow ribbon of albite in the margin (An<sub>10</sub>Ab<sub>85</sub>Or<sub>5</sub>, Table 2a, Figs. 2c and 3a), which

supports the petrographic investigations (Fig. 3d). The average Or content of potassium feldspar

crystals in altered and unaltered rocks ranged from Or<sub>84</sub> to Or<sub>96</sub>, respectively.

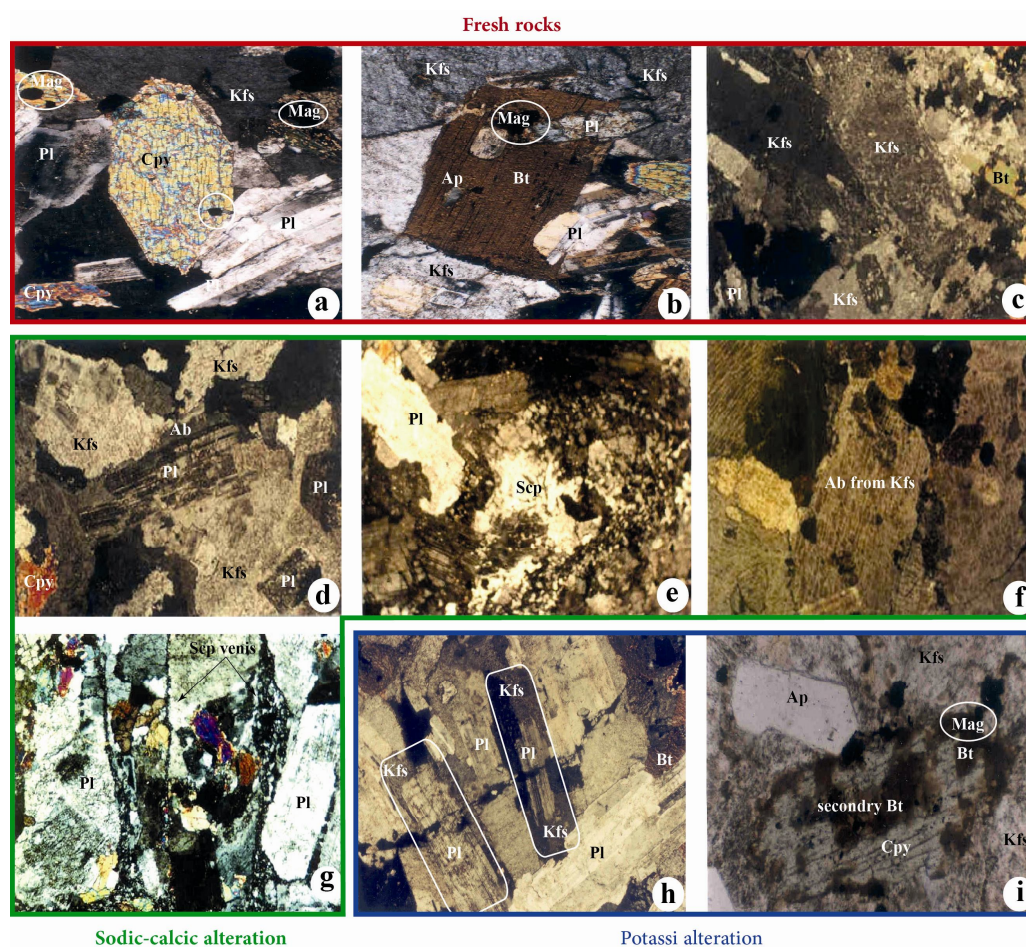


Figure 2: Petrographic features of different rocks from the Panj-Kuh pluton. a) Mineral assemblages and granular texture from fresh pyroxene syenites (Xpl, 25x); b) magmatic biotite, contains apatite and opaque inclusions in biotite syenites (Xpl, 25x); c) coarse-grained K-feldspar with Carlsbad twinning and perthitic texture, which implies its magmatic origin (Xpl, 10x); d) medium- to coarse-grained monzonite associated with albization of plagioclase in the margin (Xpl, 25x); e) occurrence of scapolite from plagioclase and full or partial removal of magnetite in monzonite (Xpl, 40x); f) preserved cleavage traces in feldspar in monzonite, which displays albization of K-feldspar; g) presence of scapolite veins with starting sodic-calcic alteration (Xpl, 40x); h) plagioclase replaced by secondary K-feldspar; note the Carlsbad twinning around plagioclases (Xpl, 25x); i) secondary biotite with pale green brown pleochroic at the expense of pyroxene (Ppl, 100x). The coloured boxes show petrographic evidence of fresh, sodic-calcic and potassic alterations (abbreviations are after Kretz, 1983).

### Scapolite

Eight electron microprobe analyses were conducted of scapolite in Na-Ca altered rocks (Table 2b, #3). Scapolite has a marialite content ( $\text{Na}_4\text{Al}_3\text{Si}_9\text{O}_{24}\text{Cl}$ ) of between 86% and 97%. The extensive distribution of this mineral at the end-northern-margin of the pluton and as corridors in the central parts of the pluton body suggests regional Na-Cl metasomatism related to igneous activity (Frietsch *et al.*, 1997). This type of alteration, in addition to the presence of scapolite and albite, is commonly associated with significant Fe-oxide Cu-Au deposits (Williams *et al.*, 1999).

### Biotite

Two distinct types of biotite were petrographically distinguished: 1. dark brown euhedral crystals with textural relationships that suggest they were probably formed early and were magmatic in origin; 2. colourless to light-brown aggregates that is pseudomorph of pyroxene or magmatic biotite and were likely of potassic-hydrothermal origin. In total, six electron microprobe analyses were conducted of book biotites from one biotite syenite (Table 2c, #1).

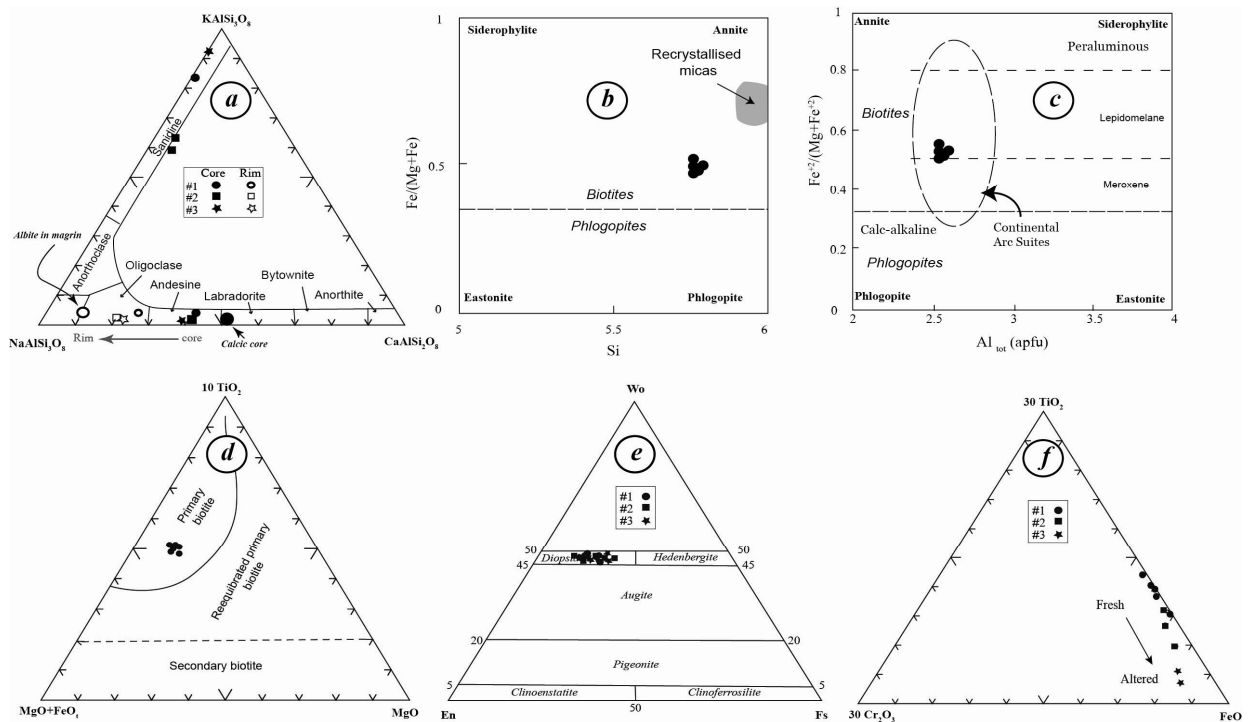


Figure 3: Chemical compositions and nomenclature of some minerals from different rock types in the Panj-Kuh intrusive body. a) Compositional variations of plagioclase and K-feldspar phenocrysts from core to rim in fresh to intense sodic-calcic altered rocks; b) classification diagram for biotite (Rieder *et al.*, 1998) in the biotite syenite; c) biotite composition plotted on continental arc suite (Tröger, 1982); d) discrimination diagram between primary magmatic biotites, re-equilibrated biotites and neoformed biotites (Nachit *et al.*, 2005); e) composition ranges and nomenclature for the Ca-Mg-Fe clinopyroxenes (Deer *et al.*, 1962); f) chemical compositional changes of magnetite from fresh- to sodic-calcic altered rocks.

As expected from petrographic observations and according to a diagram by Nachit *et al.* (2005), they had a magmatic origin (Fig. 3d). The  $Mg/(Mg + Fe^{2+})$  of the analysed biotites at Panj-Kuh ranged from 0.53 to 0.55. The analysed compositions were clustered near the vertical dashed line at  $Fe/(Fe+Mg) = 0.33$ . Mason (1993) used this value to distinguish biotite ( $>0.33$ ) from phlogopite. Although no analysis was done on shreddy biotites to prove its hydrothermal origin, some researches (e.g., Doucette, 2000) have shown that magmatic biotite has  $Fe/(Fe+Mg)$  ratios lower than 0.33; therefore, this ratio cannot be considered an unequivocal method for distinguishing between igneous and metasomatic biotites. Therefore, optical properties are the best criteria for discrimination in this case.

### Pyroxene

In total, 57 pyroxenes as the primary mafic mineral were determined in three separate samples. The averages of these samples are summarized in Table 2d. The electron microprobe analyses of pyroxenes from the Panj-Kuh pluton are clearly plotted within

the calcium pyroxene fields of diopside ( $CaMgSi_2O_6$ ) and hedenbergite ( $CaFeSi_2O_6$ ) on the Ca-Mg-Fe pyroxene classification diagram (Fig. 3e). Its average composition in the fresh biotite syenite and Na-Ca altered rocks is comparable and ranges from  $Wo_{48}En_{38}Fo_{12}$  to  $Wo_{47}En_{39}Fo_{13}$  (Table 2d, Fig. 3e). The present results show that secondary Na-Ca hydrothermal effects do not tend to alter the composition of primary clinopyroxenes.

### Accessory minerals

The principal opaque mineral of the least altered rocks was magnetite. Exsolution lamellae of ilmenite were also observed in the magnetite crystals of a few thin sections (Table 2e, #1). The anhedral shapes of the crystal clusters of hydrothermal magnetite were considerably different from the characteristic cubic pattern of the magmatic variety. These may have originated as resorption products of the magmatic magnetite and were therefore the result of a hydrothermal process. Microprobe analyses of both types of magnetite are given in Table 2e and are plotted on a ternary diagram ( $TiO_2$ - $FeO$ - $Cr_2O_3$ ) in Figure 3f. In this

graph, hydrothermal magnetite is distinguishable in composition from that with magnetic origin; there are systematic variations in minor element compositions of iron oxides, so that the content of Fe and Cr in the oxides decreased and Ti content increased from the fresh sample (syenite, #1) to more Na-Ca altered rocks (monzonites, samples 2 and 3). The analysis of magnetite grains indicates a nearly pure  $\text{Fe}_3\text{O}_4$  composition.

Apatite was present in altered and unaltered rocks of the Panj-Kuh pluton. It exhibited two distinctly different sizes and habits: 1. as tiny rod-shaped crystals that were typically less than 0.01 mm in length; 2. as stout crystals with circular cross-sections, which were as large as one millimetre in diameter. The analysed apatites were classified as fluor-apatites with F content between

4.5 and 5.4 wt% (Table 2f). REE were not detected. The common association of sphene with mafic minerals, apatite and magnetite, as well as the inclusion of these minerals within one another, suggests that they formed contemporaneously.

#### *Alteration, mineralization and mass changes*

In the Panj-Kuh area, Fe skarn deposits were formed largely in Eocene volcanic rocks (consisting of porphyritic andesite, Fig. 4a) near contact with intrusive rocks at latitude  $35^{\circ} 47' \text{N}$  and longitude  $54^{\circ} 26' \text{E}$  (Fig. 2). The deposits generally comprised magnetite as the principal ore mineral and less than 5% chalcopyrite, pyrite or hematite, which were surrounded by combinations of diopside, epidote, actinolite, chlorite, calcite and quartz (Figs. 4b and c).

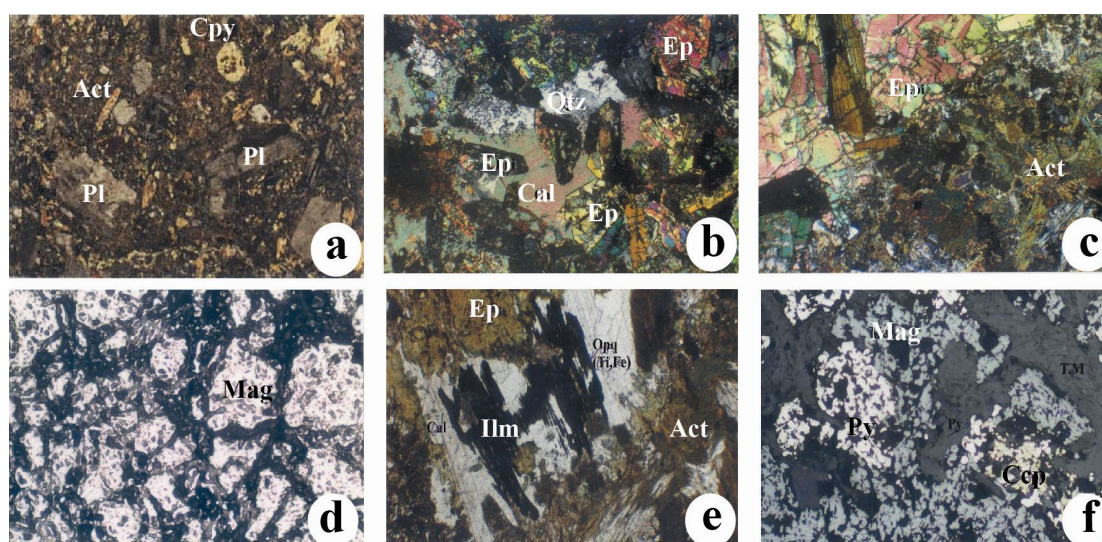


Figure 4: Textural and mineral associations typical of the Panj-Kuh iron ore deposit. a) Fresh andesite-porphyritic rocks host iron ore deposits (Xpl, 25x); b) association of epidote, actinolite, calcite and quartz as the main gangue minerals in iron deposits (Xpl, 33x); c) actinolite-filled fracture- cutting magnetite ore (Xpl, 33x); d) coarse-grained magnetite with disseminated texture as the main constitute of ore in reflected light (Xpl, 200x); e) lamella minerals appear to be titanomagnetite, surrounded by epidote-actinolite-calcite grandmass (Xpl, 33x); f) magnetite (grey), pyrite (white) and chalcopyrite (yellow) in reflected light (Xpl, 200x).

In polished sections, magnetite was often massive, poikiloblastic and very pale pinkish to brown-grey, and completely isotropic, and therefore interpreted as being of hydrothermal origin (Fig. 4d). Hematite also developed in magnetite as exsolution lamella (Fig. 4e) and presented in the upper part of the mineralized bodies, grading in colour from reddish-ochre to steel-grey. The ratio of hematite to magnetite decreased with depth. In addition, pyrite and chalcopyrite as the main sulphide phases in subordinate amounts (about 5% wt) accompanied magnetite (Fig. 4f). Clinopyroxene, pale green and mostly fine-grained,

commonly occurred as shattered, short prismatic or anhedral crystal and sometimes exhibited a granoblastic texture. The abundance of clinopyroxene (diopside-hedenbergite) increased markedly when approaching skarn contact. Amphibole, such as tremolite and actinolite, were the principal hydrous mineral and in hand specimens, occurred as aggregates forming patches or zones intergrown with magnetite or in veins (Fig. 4c). This mineral is late silicate mineral, which replaced clinopyroxene or was accompanied by sulphides such as chalcopyrite. Epidote occurred as envelopes on skarn veins and disseminated in

surrounding volcanic rocks. This mineral is commonly found together with amphibole, quartz and calcite within fractures.

According to Hitzman *et al.* (1992), extensive alteration occurs in the host rocks of iron deposits, but the alteration mineralogy and intensity may vary considerably, both within and between districts, depending on the host lithology and depth of formation. On the other hand, Na-rich hydrothermal alteration has long been recognized as a feature of many Fe-oxide-rich hydrothermal systems (Lindgren, 1913). Na-Ca hydrothermal alteration and mineralization in the Panj-Kuh area is concentrated on the intrusive body and were broadly synchronous with its emplacement. Early hydrothermal alteration was dominantly sodic-calcic and was followed by potassic alteration. Rocks that have undergone sodic-calcic alteration showed a bleached appearance and were depleted of ferromagnesian silicates. Sodic feldspar, after K-feldspar, was commonly chessboard-patterned, indicating its replacement origin. Scapolitization and albitization of the corners of plagioclase were also common. All of these features were observed in monzonitic rocks within intrusive rock in the Panj-Kuh district. As previously noted, the amount and intensity of sodic-calcic alteration increased toward the ore body (Fig. 1). The observed potassic altered rocks in the west-end were accompanied to minor Cu mineralization (Fig. 1). These rocks were principally characterized by the development of secondary (shreddy) biotite after clinopyroxene and book biotite, as well as the local replacement of plagioclase by secondary K-feldspar (Figs. 2i and h). In the present study, which excepted petrographical evidence, unfortunately, there was no chemical analysis conducted for rocks undergoing potassic alteration.

The following section describes geochemical variations as a function of crystallization and Na-Ca alteration in the studied intrusive rocks. The initial concentrations of Rb, Sr and Ba in such rocks were controlled by processes of fractional crystallization and were dependent on their relative partition coefficients (Rollinson, 1993). This means that concentrations of Sr and Ba decreased, while Rb increased in residual fluids with increasing crystallization. On the other hand, the element pairs K-Rb, K-Ba and Ca-Sr, respectively, had similar ionic properties. Therefore, Rb and Ba are usually substituted in potassic minerals such as K-feldspar

and biotite, and is Sr-substituted in minerals such as plagioclase. In this context, plots of Ba vs. Rb or Sr vs. Rb are very sensitive to crystal fractionation. The plots presented in Figures 5a, b and c indicate crystal fractionation and proposed alteration trends as determined by geochemical analyses for plutonic rocks of the studied area.

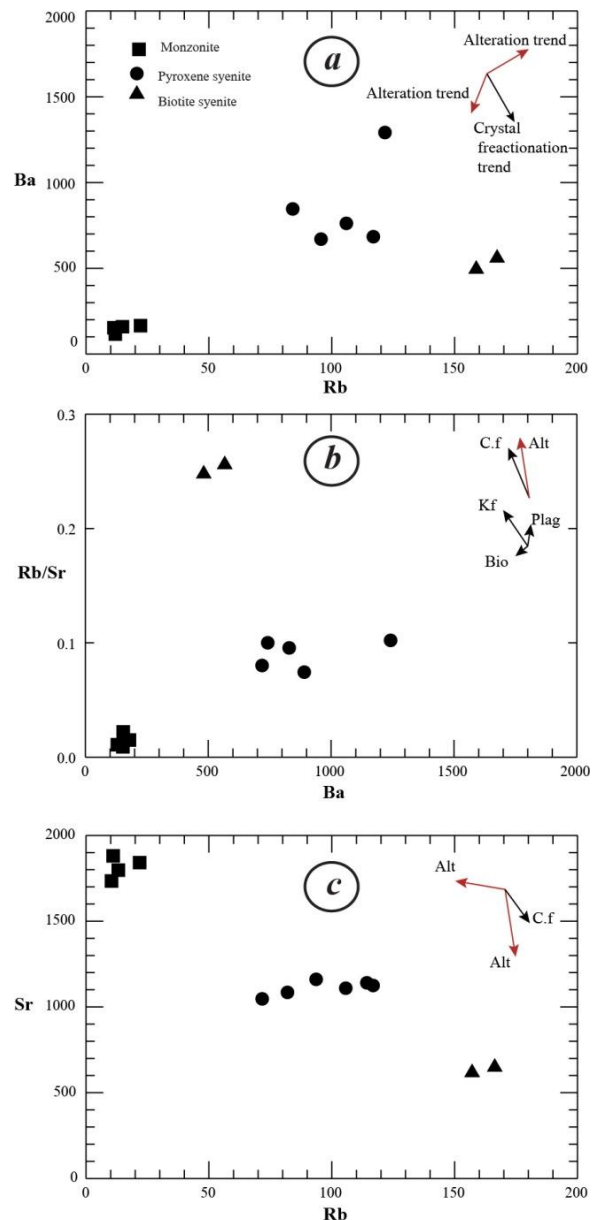


Figure 5: Bivariate plots of Ba vs. Rb (a), Rb/Sr vs. Ba (b) and Sr vs. Rb (c) with indicated crystal fractionation trends and alteration trends.

Similarities between alteration and fractionation trends in Figure 5b was interpreted to be dependent on the primary mineral phase involved in both processes, i.e., the feldspars. The fractionation

trend was considered distinct from that of the sodic-calcic trend. During the fractionation process and the resultant growth of K-feldspar and biotite, an increase in Rb/Sr and decrease in Ba might be expected. With sodic-calcic metasomatism and conversion of K-feldspar to albite, and the resulting new scapolite and albite, the amount of Rb/Sr and Ba decreased. The positions of fresh and altered samples plotted in Figure 5 corresponded with this prediction and the accompanying Rb and Ba decrease may correspond to the reduction of K-feldspar in the altered assemblage.

In this study, mass gains and losses during Na-Ca alteration were calculated using Grant's (1986) isocon method. The first step in this technique is to identify the pre-alteration composition of an altered rock. By carefully consideration of the field relations and petrographic characteristics of the local geologic setting, an average of three of the least-altered pyroxene syenite samples were selected as reference mass of the original sample (#PySy\* in Table 3, assigned a value of 100 grams).

Table 3: Geochemical data for the fresh rocks used to estimate variation mass changes.

Type	Fresh						Molecular proportions						Range	Average
	1	2	3	4	5	6	1	2	3	4	5	6		
Number	Py-	Py-	Py-	Bi-	Bi-	Bi-	Py-Sy	Py-Sy	Py-Sy	Bi-Sy	Bi-Sy	Bi-Sy		
Sample	Py-	Py-	Py-	Bi-	Bi-	Bi-	Py-Sy	Py-Sy	Py-Sy	Bi-Sy	Bi-Sy	Bi-Sy		
g/100g														
SiO <sub>2</sub>	54.39	53.83	54.92	56.91	56.98	56.06	62.52	62.47	63.72	69.78	67.30	66.88	1.25	62.90
TiO <sub>2</sub>	0.70	0.75	0.70	0.45	0.50	0.48	0.61	0.65	0.61	0.41	0.44	0.43	0.05	0.62
Al <sub>2</sub> O <sub>3</sub>	18.54	17.79	17.60	16.52	18.20	18.16	12.56	12.16	12.03	11.94	12.66	12.76	0.52	12.25
Fe <sub>2</sub> O <sub>3</sub>	2.59	2.58	2.54	1.37	2.34	2.27	1.12	1.13	1.11	0.63	1.04	1.02	0.02	1.12
FeO	2.71	2.78	2.59	1.45	2.02	2.06	2.60	2.70	2.51	1.49	1.99	2.05	0.18	2.60
MnO	0.06	0.08	0.06	0.03	0.06	0.09	0.06	0.08	0.06	0.03	0.06	0.09	0.02	0.07
MgO	2.42	2.82	2.55	1.17	1.28	1.35	4.15	4.88	4.41	2.14	2.25	2.40	0.73	4.48
CaO	5.50	5.19	4.69	2.56	2.38	2.63	6.77	6.45	5.83	3.36	3.01	3.36	0.94	6.35
Na <sub>2</sub> O	4.68	4.48	4.35	5.28	5.31	5.12	5.21	5.04	4.89	6.28	6.08	5.92	0.32	5.05
K <sub>2</sub> O	5.76	5.71	6.28	4.90	6.71	6.52	4.22	4.23	4.65	3.83	5.05	4.96	0.42	4.37
P <sub>2</sub> O <sub>5</sub>	0.38	0.43	0.36	0.21	0.21	0.24	0.18	0.21	0.18	0.11	0.10	0.12	0.03	0.19
g/1000kg														
Cr	67	49	47	95	52	68	47.66	34.81	33.72	70.88	47.08	66.35	13.94	38.73
Ni	16	21	20	8	14	10	10.03	13.15	12.65	5.26	11.17	8.60	3.12	11.94
Co	9.40	11.80	10.60	3.40	8.30	7.90	5.89	7.39	6.70	2.24	6.62	6.79	1.49	6.66
Sc	11	11	11	5	6	6	8.14	8.13	8.21	3.88	5.65	6.09	0.08	8.16
V	143	145	134	63	68	71	103.7	105.0	98.01	47.93	62.78	70.63	7.01	102.25
Rb	93.70	120	108	78.90	167	156	40.77	52.15	47.40	36.01	92.51	93.12	11.38	46.77
Cs	1.70	2.50	2.30	0.70	3.80	3.60	0.47	0.69	0.65	0.20	1.35	1.37	0.22	0.60
Ba	658	676	773	868	579	471	177.6	182.2	210.4	245.8	198.9	174.4	32.83	190.13
Sr	1180	1160	1110	1090	651	633	495.9	486.9	470.5	480.5	348.3	364.9	25.43	484.46
Ga	20	19	20	22	21	21	10.57	10.03	10.66	12.19	14.13	15.22	0.63	10.42
Ta	0.80	0.80	0.80	0.80	1.40	1.20	0.16	0.16	0.16	0.17	0.36	0.34	0	0.16
Nb	15	14	14	14	24	20	5.97	5.56	5.62	5.84	12.15	10.91	0.40	5.71
Hf	4	3	3	3	6	5	0.83	0.62	0.63	0.65	1.59	1.43	0.21	0.69
Zr	102	97.80	118	108	221	172	41.46	39.70	48.37	46.04	114.3	95.90	8.67	43.18
Ti	0.42	0.45	0.42	0.27	0.30	0.29	0.32	0.35	0.33	0.22	0.29	0.31	0.02	0.33
Y	20	20.40	20.10	12.70	22.20	20.20	8.32	8.48	8.43	5.54	11.76	11.53	0.16	8.41
Th	11.20	9.10	11.40	9.60	21.10	15.70	1.79	1.45	1.83	1.61	4.28	3.43	0.38	1.69
U	2.53	2.14	2.62	2.28	4.93	3.65	0.39	0.33	0.41	0.37	0.98	0.78	0.08	0.38
La	32.70	37.10	27.80	24.80	51.10	48.70	8.70	9.86	7.46	6.92	17.31	17.78	2.40	8.67
Ce	73.30	77.40	61.20	59.10	95.70	90.30	19.35	20.40	16.29	16.36	32.16	32.70	4.11	18.68
Nd	32	34.50	30.60	29.70	35.60	35.40	8.21	8.84	7.91	7.99	11.62	12.45	0.92	8.32
Sm	6.30	6.40	6.10	5.70	6	6	1.55	1.57	1.51	1.47	1.88	2.02	0.06	1.55
Eu	1.46	1.60	1.57	1.74	1.29	1.38	0.36	0.39	0.39	0.44	0.40	0.46	0.03	0.38
Gd	5.73	5.73	5.31	4.63	5.42	5.41	1.35	1.35	1.26	1.14	1.62	1.75	0.09	1.32
Yb	2	1.90	1.90	1.20	2.40	2.30	0.43	0.41	0.41	0.27	0.65	0.67	0.02	0.41

These samples contained plagioclase, pyroxene and less or no biotite, minor magnetite, as well as apatite and sphene, which are characteristic of the majority of the least altered igneous rocks. It was used as a reference material for the geochemical modelling presented below. The elements Ti and REE are commonly immobile during hydrothermal alteration and have mostly been used as the basis of mass balance calculation in many porphyry copper deposits (Ulrich and Heinrich, 2001; Hezarkhani, 2002; Arifudin, 2006). According to MacLean and Kranidiotis (1987), the correlation coefficient of chemically unrelated elements against one another ( $r$ ) is used to estimate the relative immobility of one element with respect to another. Therefore, Ti and REEs were interpreted as relatively immobile elements in the sodic-calcic alteration and were selected as mass change indicators in this study.

Isocon diagrams were prepared by plotting the oxide and element values of a least-altered rock against the same values for the samples of altered rocks. It means that the concentration of a particular oxide or element is multiplied by a factor for both the unaltered and altered rock, in order to construct a line of best fit for immobile elements (the isocon) on a dimensionless plot of unaltered versus altered rock.

The gains and losses of chemical constituents were estimated by determining the difference between the predicted concentration of an element or oxide in grams per 100 grams of rock, or ppm, taken from an isocon and that of an altered sample. Mass changes for unaltered and sodic-calcic altered intrusive rocks from the Panj-Kuh pluton, based on a constant volume assumption, are shown in Table 3. Comparisons of sample M\* (average composition of the sodic-calcic rocks) with the least-altered sample, PySy\*, showed that most immobile elements such as Ce, Yb and TiO<sub>2</sub> plotted close to or on a line of constant mass with a slope of 0.96 (Fig. 6).

However, the element Eu, which is generally considered to be geochemically immobile, plotted off the line, possibly due to the presence in feldspars. It is clear that the Na-Ca altered rocks gained Na, Ca, Cs, Sr, Zr and Cr and lost K, Rb, Ba, Co and Ni. Mass changes associated with sodic alteration for five samples are presented numerically in Table 5. As expected from the sum of losses and gains, mass changes varied according to the intensity of alteration. This finding agreed

with the variation of mineral assemblage in the sodic-calcic alteration zone (appearance of scapolite, albite, conversion of K-feldspar to plagioclase at the expense of dissolution and removal of magnetite). Contrastingly, K, Fe and a small amount of copper were added to potassically-altered rocks. The latter element could be inferred from the dissemination of malachite and azurite in the potassically-altered zone. In fact, the increase of Cu is consistent with the mobilization of this element and its concentration mainly in Cu-carbonates, and rarely in disseminated sulphide minerals.

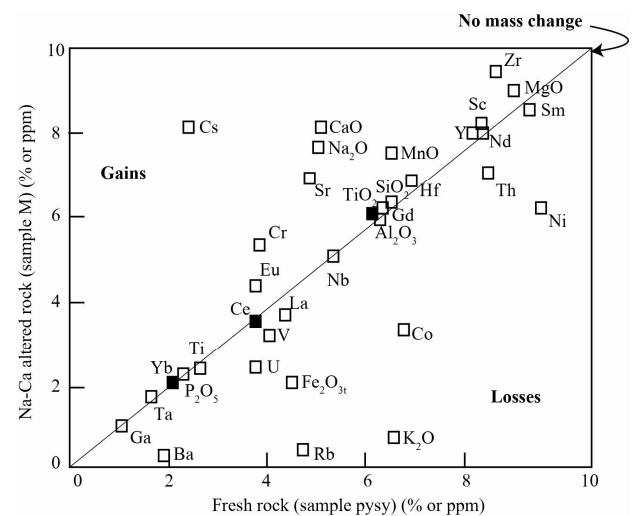


Figure 6: An isocon diagram comparing a representative sample of the sodic-calcic alteration samples (M\*) with a representative sample of least-altered rock (Py-Sy\*). The dashed line (isocon) is drawn for the largest number of potentially immobile elements (solid squares).

## Conclusion

Detailed field-mapping of wall-rock alteration and veinlets, combined with petrographic and mineral compositions in the Panj-Kuh pluton show crystal fractionation from pyroxene syenite in the margins to biotite syenite in the centre and western margins. These rocks have been converted through a series of reactions to two hydrothermal associations referred to as sodic-calcic and potassic alterations. These associations include only hydrothermally introduced minerals and primary magmatic minerals that have remained stable during alteration. Monzonites, which have the highest Na<sub>2</sub>O, CaO content, are the result of pervasive sodic-calcic alteration and are characterized by 1. a lightened appearance; 2. scapolitization of plagioclase; 3. K-feldspar replaced by Na

plagioclase; 4. plagioclase rinds of albite; 5. leaching of magnetite. Scapolite forms porphyroblasts, smaller individual grains that together with albite and analcime, replace plagioclase and veins. The regional extent of sodic-calcic alteration associated with all iron-oxide copper-gold IOCG deposits confirms transportation of Fe in fluid flow, as well as the deposition mechanisms of iron oxides. Mass changes in the major and trace elements associated with Na-Ca altered rocks show that the aluminium, Ga, Ti and REEs are reliably immobile. Consistent gains in Na, Ca, Cs and Sr are matched by depletions in K, Ba, Rb and Fe. The latter elements are being very

mobile (depleted) in intensely altered rocks and are released to the fluid. Leached elements are those that are specifically enriched in the potassic alteration zone of the Fe and in proximal Cu ore indication.

#### Acknowledgments

I am grateful to Anna Maria Fioretti for the electron microprobe analyses conducted at CNR- IGG (Padua-Italy). The Smithsonian Natural History Museum is thanked for providing the Smithsonian Microbeam Standards for microprobe analyses.

#### References

- Alavi, M., 1972. Etude géologique de la région de Djam, Geological Survey of Iran, Report: No.23.
- Arifudin, A., 2006. Petrology, geochemistry and compositional changes of diagnostic hydrothermal minerals within the Batu Hijau porphyry copper-gold deposit, Sumbawa Island, Indonesia: Ph.D thesis, University of RWTH Aachen.
- Barton, M. D., Johnson, D. A., 2000. Alternative brine sources for Fe-oxide (-Cu-Au) systems: Implications for hydrothermal alteration and metals, In: Porter, T.M. (Eds.), Hydrothermal iron oxide copper-gold and related deposits, a global perspective. Australian Mineral Foundation, Glenside, South Australia, pp. 43-60.
- Carten, R.B., 1982. Sodium – calcium metasomatism: Chemical, temporal and spatial relationship at Yerington, Nevada, porphyry copper deposit. *Economic Geology*, 81: 1495-1519.
- Deer, W. A., Howie R. A, Zussman J., 1962. Sheet silicates. In: Rock forming minerals 3, 270 p. Longmans, Green and Co., London.
- Dilles, J. H., 1984. The petrology and geochemistry of the Yerington batholith and the Ann – Mason Porphyry Copper deposit, Western Nevada: Ph. D. thesis, University of Stanford.
- Doucette, J., 2000. A Petrochemical Study of the Mount Fubilan Intrusion and Associated Ore Bodies, Papua New Guinea. Ph.D. thesis, University of Oregon State.
- Droop, G.T.R. 1987. A general equation for estimating Fe<sup>3+</sup> concentrations in ferromagnesian silicates and oxides from microprobe analyses, using stoichiometric criteria, *Mineralogical Magazine*, 51: 431-435.
- Gilluly, 1993. Replacement origin of the albite granite near the Sparat, Orogen. *United State Geological Survey*, 175: 65-81.
- Grant, J. A., 1986. The isocon diagram - a simple solution to Gresens' equation for metasomatic alteration. *Economic Geology*, 81: 1976-1982.
- Hezarkhani, A., 2002. Mass changes during hydrothermal alteration/mineralization in a porphyry copper deposit, eastern Sungun, northwestern Iran. *Journal of Asian Earth Science*, 20: 567-588.
- Hitzman, M. W., Oreskes N., Einaudi, M. T., 1992. Geological characteristic and tectonic setting of Proterozoic iron oxide (Cu- Au- REE) deposits, *Precambrian Research*, 58: 241-287.
- Kretz, R., 1983. Symbols for rock-forming minerals. *American Mineralogist*, 68: 277-279.
- Lindgren, W., 1913. *Mineral deposits*, McGraw-Hill, New York , 930 pp.
- MacLean, W.H., Kranidiotis, P., 1987. Immobile elements as monitors of mass transport in hydrothermal alteration: Phelps Dodge massive sulphide deposit, Matagami. *Economic Geology*, 82: 951-962.
- Mason, D., R., 1993. Petrological Studies of a Suite of Rock Samples From The Ok Tedi Mine, Papua New Guinea Part II -Biotite Analyses And Clay Identifications. Amdel Laboratories, Report G692300G/93.
- Meinert, L. D., 1995. Igneous petrogenesis and skarn deposits, *Geological Association of Canada, Special paper*, 40: 569-583.
- Nachit, H., Ibhi A., Abia E. L. H., Ohoud M. B., 2005. Discrimination between primary magmatic biotites, re-equilibrated biotites and neoformed biotites. *Les Comptes Rendus de l'Académie des sciences. Paris Geoscience*, 337: 1415-1420.
- Papike, J.J. (Eds.) 1969. *Pyroxene and Amphibole: crystal chemistry and phase petrology*, Mineralogical Society of America Special Paper, n. 2.
- Sokolova, E., Hawthorne, F. 2008. The crystal chemistry of the scapolite-group minerals. I. Crystal structure and long-range order. *Canadian Mineralogist*, 46: 1527-1554.
- Pouchou, J. L., Pichoir, F. 1991. Quantitative analysis of homogeneous or stratified microvolumes applying the model

- “PAP”. In: Electron Probe Quantitation, Heinrich, K.F.J. & Newbury, D.E. (Eds.), Plenum Press, New York, 31 - 75.
- Rieder, M., Cavazzini, G., D`Yakonov, Y.S., Frank-Kamentskii, V.A., Gottardi, G., Guggenheim, S., Koval, P.V., Müller, G., Neiva, A.M.R., Radoslovich, E.W., Robert, J-L., Sassi, F.P., Takeda, H., Weiss, Z., Wones, D.R., 1998. Nomenclature of the micas. *The Canadian Mineralogist*, 36: 41-48.
- Rollinson, H. R., 1993. Using geochemical data. evaluation, presentation, Longman, 352 pp.
- Sheibi, M., 2003. Petrology and geochemistry of intrusive rocks and iron Skarn of Panj-Kuh (South east of Damghan, MSc. thesis, University of Tehran.
- Tröger, W.E., 1982. Optische Bestimmung der gesteinsbildenden Minerale. Teil 2. Schweizerbartsche Verlagsbuchhandlung, Stuttgart. 822 pp.
- Ulrich, T., C. Henric, C. A., 2001. Geology and alteration geochemistry of the porphyry Cu-Au deposit at Bajo de la Alumbrera, Argentina. *Economic Geology*, 96: 1719-1742.
- Van Middelaar, W.T., Keith, J. D., 1990. Mica chemistry as an indicator of Oxygen and halogen fugacities in the Cantung and other related granitoids in the North American Cordillera., In: Stein, H., J. and Hannah, J. L. (Eds.), 1990. Ore – bearing granite systems, Petrogenesis and mineralizing Processes. Geological Society of America, Special Paper, 246pp.
- Williams, P. J., Dong, G., Pollard, P. G., Perring, C. S., 1999. Fluid inclusion geochemistry of Cloncurry (Fe-Cu-Au deposits). In: Stanley, C. J. (Eds.) Mineral deposits: Processing: Rotterdam, Balkema, pp. 111-114.